Research Article | Vol. 24, No. 25 | 12 Dec 2016 | OPTICS EXPRESS 28540

Optics EXPRESS

Compact, lensless digital holographic microscope for remote microbiology

EUGENE SERABYN,[1,*] KURT LIEWER,[1] CHRIS LINDENSMITH,[1] KENT WALLACE,[1] AND JAY NADEAU[2]

[1]*Jet Propulsion Laboratory, California Institute of Technology, 4800 Oak Grove Drive, Pasadena, CA 91109, USA*
[2]*Graduate Aerospace Laboratories, California Institute of Technology, 1200 E. California Blvd., Pasadena, CA 91125, USA*
[*]*gene.serabyn@jpl.nasa.gov*

Abstract: *In situ* investigation of microbial life in extreme environments can be carried out with microscopes capable of imaging 3-dimensional volumes and tracking particle motion. Here we present a lensless digital holographic microscope approach that provides roughly 1.5 micron resolution in a compact, robust package suitable for remote deployment. High resolution is achieved by generating high numerical-aperture input beams with radial gradient-index rod lenses. The ability to detect and track prokaryotes was explored using bacterial strains of two different sizes. In the larger strain, a variety of motions were seen, while the smaller strain was used to demonstrate a detection capability down to micron scales.

OCIS codes: (090.1995) Digital holography; (100.3175) Interferometric imaging; (120.4570) Optical design of instruments.

References and links

1. B. Sherr, E. Sherr, and P. del Giorgio, "Enumeration of total and highly active bacteria," Methods Microbiol. **30**, 129–159 (2001).
2. J. G. Mitchell and K. Kogure, "Bacterial motility: links to the environment and a driving force for microbial physics," FEMS Microbiol. Ecol. **55**(1), 3–16 (2006).
3. K. Son, D. R. Brumley, and R. Stocker, "Live from under the lens: exploring microbial motility with dynamic imaging and microfluidics," Nat. Rev. Microbiol. **13**(12), 761–775 (2015).
4. J. Nadeau, C. Lindensmith, J. W. Deming, V. I. Fernandez, and R. Stocker, "Microbial morphology and motility as biosignatures for outer planet missions," Astrobiology **16**(10), 755–774 (2016), doi:10.1089/ast.2015.1376.
5. N. Thomas, B. S. Lüthi, S. F. Hviid, H. U. Keller, W. J. Markiewicz, T. Blümchen, A. T. Basilevsky, P. H. Smith, R. Tanner, C. Oquest, R. Reynolds, J.-L. Josset, S. Beauvivre, B. Hofmann, P. Rüffer, and C. T. Pillinger, "The microscope for Beagle 2," Planet. Space Sci. **52**(9), 853–866 (2004).
6. K. S. Edgett, R. A. Yingst, M. A. Ravine, M. A. Caplinger, J. N. Maki, F. T. Ghaemi, J. A. Schaffner, J. F. Bell III, L. J. Edwards, K. E. Herkenhoff, E. Heydari, L. C. Kah, M. T. Lemmon, M. E. Minitti, T. S. Olson, T. J. Parker, S. K. Rowland, J. Schieber, R. J. Sullivan, D. Y. Sumner, P. C. Thomas, E. H. Jensen, J. J. Simmonds, A. J. Sengstacken, R. G. Willson, and W. Goetz, "Curiosity's Mars Hand Lens Imager (MAHLI) Investigation," Space Sci. Rev. **170**(1-4), 259–317 (2012).
7. M. K. Kim, *Digital Holographic Microscopy Principles, Techniques, and Applications* (Springer, 2011).
8. S. Seo, T.-W. Su, D. K. Tseng, A. Erlinger, and A. Ozcan, "Lensfree holographic imaging for on-chip cytometry and diagnostics," Lab Chip **9**(6), 777–787 (2009).
9. O. Mudanyali, D. Tseng, C. Oh, S. O. Isikman, I. Sencan, W. Bishara, C. Oztoprak, S. Seo, B. Khademhosseini, and A. Ozcan, "Compact, light-weight and cost-effective microscope based on lensless incoherent holography for telemedicine applications," Lab Chip **10**(11), 1417–1428 (2010).
10. J. K. Wallace, S. Rider, E. Serabyn, J. Kühn, K. Liewer, J. Deming, G. Showalter, C. Lindensmith, and J. Nadeau, "Robust, compact implementation of an off-axis digital holographic microscope," Opt. Express **23**(13), 17367–17378 (2015).
11. C. A. Lindensmith, S. Rider, M. Bedrossian, J. K. Wallace, E. Serabyn, G. M. Showalter, J. W. Deming, and J. L. Nadeau, "A submersible, off-axis holographic microscope for detection of microbial motility and morphology in aqueous and icy environemnts," PLoS One **11**(1), e0147700 (2016).
12. G. W. Stroke, "Lensless Fourier-transform method for optical holography," Appl. Phys. Lett. **6**(10), 201–203 (1965).
13. W. S. Haddad, D. Cullen, J. C. Solem, J. W. Longworth, A. McPherson, K. Boyer, and C. K. Rhodes, "Fourier-transform holographic microscope," Appl. Opt. **31**(24), 4973–4978 (1992).

#276105 http://dx.doi.org/10.1364/OE.24.028540
Journal © 2016 Received 20 Sep 2016; revised 21 Nov 2016; accepted 21 Nov 2016; published 1 Dec 2016

Optics EXPRESS

14. W. Xu, M. H. Jericho, I. A. Meinertzhagen, and H. J. Kreuzer, "Digital in-line holography for biological applications," Proc. Natl. Acad. Sci. U.S.A. **98**(20), 11301–11305 (2001).
15. L. Repetto, E. Piano, and C. Pontiggia, "Lensless digital holographic microscope with light-emitting diode illumination," Opt. Lett. **29**(10), 1132–1134 (2004).
16. U. A. Gurkan, S. Moon, H. Geckil, F. Xu, S. Wang, T. J. Lu, and U. Demirci, "Miniaturized lensless imaging systems for cell and microorganism visualization in point-of-care testing," Biotechnol. J. **6**(2), 138–149 (2011).
17. S. O. Isikman, W. Bishara, S. Mavandadi, F. W. Yu, S. Feng, R. Lau, and A. Ozcan, "Lens-free optical tomographic microscope with a large imaging volume on a chip," Proc. Natl. Acad. Sci. U.S.A. **108**(18), 7296–7301 (2011).
18. C. Zuo, J. Sun, J. Zhang, Y. Hu, and Q. Chen, "Lensless phase microscopy and diffraction tomography with multi-angle and multi-wavelength illuminations using a LED matrix," Opt. Express **23**(11), 14314–14328 (2015).
19. W. Bishara, U. Sikora, O. Mudanyali, T. W. Su, O. Yaglidere, S. Luckhart, and A. Ozcan, "Holographic pixel super-resolution in portable lensless on-chip microscopy using a fiber-optic array," Lab Chip **11**(7), 1276–1279 (2011).
20. C. Remacha, B. S. Nickerson, and H. J. Kreuzer, "Tomography by point source digital holographic microscopy," Appl. Opt. **53**(16), 3520–3527 (2014).
21. I. Pushkarsky, Y. Liu, W. Weaver, T.-W. Su, O. Mudanyali, A. Ozcan, and D. Di Carlo, "Automated single-cell motility analysis on a chip using lensfree microscopy," Sci. Rep. **4**, 4717 (2014).
22. T.-W. Su, L. Xue, and A. Ozcan, "High-throughput lensfree 3D tracking of human sperms reveals rare statistics of helical trajectories," Proc. Natl. Acad. Sci. U.S.A. **109**(40), 16018–16022 (2012).
23. T.-W. Su, I. Choi, J. Feng, K. Huang, E. McLeod, and A. Ozcan, "Sperm trajectories form chiral ribbons," Sci. Rep. **3**, 1664 (2013).
24. K. Sato and O. Murata, "Lens-less holographic microscope with high resolving power and no-distortion," Proc. SPIE **7904**, 790402 (2011).
25. M. H. Jericho, H. J. Kreuzer, M. Kanka, and R. Riesenberg, "Quantitative phase and refractive index measurements with point-source digital in-line holographic microscopy," Appl. Opt. **51**(10), 1503–1515 (2012).
26. E. Serabyn, K. Liewer, K. Wallace, S. Rider, C. Lindensmith, and J. Nadeau "Lensless digital holgraphic microscopy for microbe detection," in *Imaging and Applied Optics 2016*, OSA Technical Digest (online) (2016), paper DTh3F.4.
27. E. Hecht, *Optics*, 4th ed. (Addison Wesley, 2002).
28. G. Pedrini and H. J. Tiziani, "Short-coherence digital microscopy by use of a lensless holographic imaging system," Appl. Opt. **41**(22), 4489–4496 (2002).
29. E. Cuche, P. Marquet, and C. Depeursinge, "Spatial filtering for zero-order and twin-image elimination in digital off-axis holography," Appl. Opt. **39**(23), 4070–4075 (2000).
30. http://www.lynceetec.com/koala-acquisition-analysis/
31. T. Colomb, "Numerical aberrations compensation and polarization imaging in digital holographic microscopy," thesis no. 3455 (Institut d'imagerie et optique appliquée, École Polytechnique Fédérale de Lausanne, 2006).
32. J. Schindelin, I. Arganda-Carreras, E. Frise, V. Kaynig, M. Longair, T. Pietzsch, S. Preibisch, C. Rueden, S. Saalfeld, B. Schmid, J. Y. Tinevez, D. J. White, V. Hartenstein, K. Eliceiri, P. Tomancak, and A. Cardona, "Fiji: an open-source platform for biological-image analysis," Nat. Methods **9**(7), 676–682 (2012).
33. K. Junge, H. Eicken, and J. W. Deming, "Motility of *Colwellia psychrerythraea* strain 34H at subzero temperatures," Appl. Environ. Microbiol. **69**(7), 4282–4284 (2003).
34. Y. Pu and H. Meng, "Intrinsic speckle noise in off-axis particle holography," J. Opt. Soc. Am. A **21**(7), 1221–1230 (2004).

1. Introduction

Conventional high-resolution microscopes capable of imaging bacteria have limited depth-of-field and typically require complex objective lenses with tight alignment tolerances. As a result, direct observation of prokaryotes (bacteria and archaea) in their native environments has yet to be performed in most parts of the Arctic and Antarctic, around hydrothermal vents, and in the majority of the open ocean [1]. Quantifying prokaryotic behavior *in situ* is important for understanding large-scale marine processes such as carbon cycling [2, 3]. It is also of great interest for the investigation of the possibility of life in extraterrestrial Ocean Worlds, such as Enceladus and Europa [4], but instruments for unambiguous detection of prokaryotes in planetary environments don't yet exist. Some microscopes have flown in space, but as yet no microscopic observations have been made on Mars with the resolution required to detect bacteria [5, 6]. For all such remote deployment scenarios, a compact, robust microscope capable of operating in an ambient environment is required.

Digital holographic microscopy [7] has a number of advantages over conventional microscopy for remote autonomous deployment, including robustness (no moving parts, as no

Optics EXPRESS

focus mechanism is needed), high throughput, and compressed sensing (i.e., the entire 3-d sample volume is encoded in each 2-d frame capture). As a result, this technique is beginning to see application beyond the laboratory [8,9]. Our previous "common path" digital holographic microscope [DHM] design [10] reported microbial imaging in Greenland sea ice [11], but its reliance on classical lens-based optics left this prototype larger than desirable for robotic deployment. On the other hand, lensless holography, with no imaging optics between the light source and detector [12–16], can enable compact, lightweight systems.

Several lensless holographic and tomographic microscope approaches exist [8,9,13–26], with differing advantages and disadvantages. For example, use of incoherent light provides speckle noise reduction [15], but also reduced fringe visibility and depth of field. Tomography [17–20] can provide high resolution, but multiple reads are needed to acquire a full information set. Conversely, motion tracking does not necessarily require high-resolution imaging [8,21]. On-chip systems can provide a large field of view (FOV) by situating the sample very close to the detector array [21–23], but thermal issues can arise from differing ambient-sample and powered-detector temperatures. A more classical lensless DHM configuration with a somewhat larger sample-to-detector distance may thus be more suited to microscopic imaging in extreme environments. Of these, laser-based systems [14, 24–26] have tended to include pinholes and additional fore-optics to increase the laser-beam numerical aperture (NA), thereby increasing system volume and alignment complexity. For robustness and compactness, ideally any difficult-to-align elements such as small pinholes should be avoided, and any high-NA laser beam (or beams) should be provided without greatly impacting system volume. This paper provides a solution to both of these issues by making use of small radial gradient-index (GRIN) rod lenses [27] to inject high NA laser beams into a lensless DHM.

2. Lensless digital holographic microscopy with GRIN lenses

In lensless holography, reference and source beams directly illuminate the detector array, without any intervening optics. However, as in standard microscopy, high-resolution holographic microscopy also requires high NA, as the linear resolution is still given by λ/(2NA). High-NA laser beams must then be launched from just in front of the detector array, i.e., from a distance, f, of ≈1 – 3 cm for a typical cm-scale array. Moreover, in the off-axis holography case, the fringes on the detector array due to the two-beam interference pattern must have a spatial period, L, of at least twice the pixel pitch, p,

$$L = f\frac{\lambda}{b} \geq 2p, \tag{1}$$

where b is the separation baseline between the two source points. For a pitch of a few μm, a roughly mm-sized source baseline is required. While a beamsplitter could be used to separate the two launch points into separate beam paths [28], in either case a number of components must be crowded together: both point sources of light (or their reimaged foci), the sample, and the camera (as well as a beamsplitter if one is employed). Launching the beams from single-mode optical fibers is an attractive possibility, as fiber tips can be located relatively freely, and unconnectorized fibers can be used to save space. However, typically available single-mode fibers have lower NAs than is necessary for μm-scale resolution, especially at shorter (blue/violet) wavelengths. The goal for off-axis holography is thus to provide, with minimal optics, a pair of high NA laser beams in close proximity to each other.

We achieve this by using small GRIN rod lenses to increase the NA of a single-mode (SM) fiber output beam. GRIN lenses with mm-scale diameters and lengths are readily available at low cost, and can be used to produce a high NA output focus from a collimated input beam [27]. A schematic of our conceptual design is shown in Fig. 1(a). A single SM fiber output beam is first collimated by a small fiber-collimating lens, and the collimated beam then over-illuminates a pair of GRIN lenses, yielding a pair of high-NA focal spots in

Optics EXPRESS

their common output plane. Illuminating both GRIN lenses with a single collimated beam removes the need for a second fiber, and makes the system common-mode until the fiber tip, thereby eliminating potential pathlength drifts to which a dual-fiber system would be susceptible. From the coplanar output foci, the two beams expand at high NA to pass through the sample and fill the camera array. With no optical elements (other than the sample) between the source pair and the detector array, the imaging stage itself is indeed lensless.

Although Fig. 1(a) shows the dual-beam off-axis DHM case, this approach can also enable a single-beam in-line DHM, by instead using only a single GRIN lens. In either case, the use of GRIN lenses eliminates the need to use or align focal-plane pinholes, as the input beam to the GRIN lens(es) is collimated. However, as is well known [7], off-axis holography enables the separation of the DC term from the real and virtual images, allowing for straightforward reconstructions of both amplitude and quantitative phase images. The latter is of great value for biological samples, many of which are transparent in amplitude. In general, off-axis holography shows a higher signal-to-noise ratio (SNR) than in-line holography because of the elimination of these images (verified in practice for our GRIN system), and so permits reconstruction in denser samples than in-line. However, in our particular dual-beam configuration, the two input beams overlap to a large extent at the sample plane, which re-introduces a second image. While this makes the study of extended objects more difficult, the overlap should not be a problem for our specific goal of searching for a sparse population of small single-cell microorganisms, as the two image planes are at opposite reconstruction distances, and so the second image will be well out of focus, and hence very faint and extended. On the other hand, the second image in effect increases the search region.

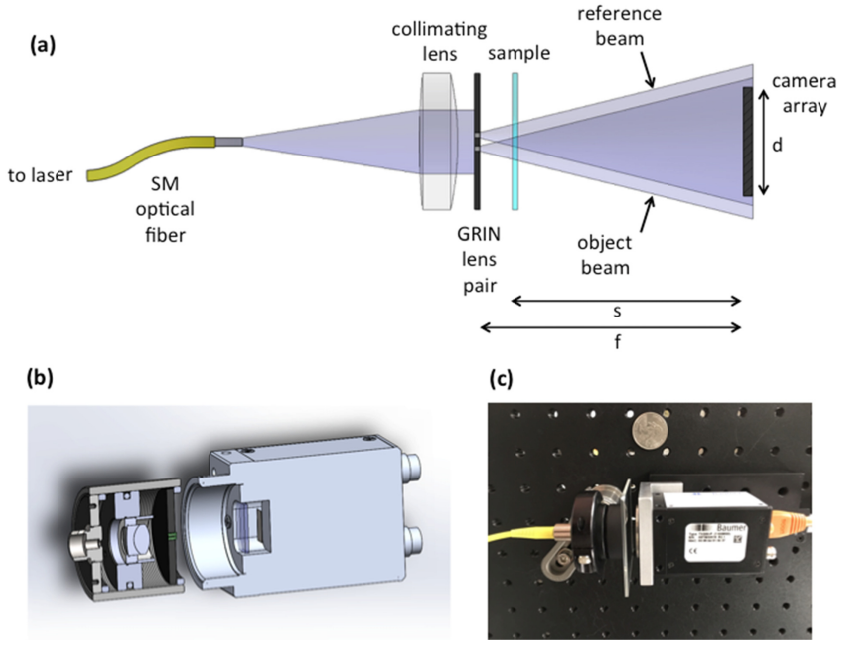

Fig. 1. (a) Schematic layout of our dual-beam off-axis DHM, (b) Solid model of our DHM, and (c) Photograph of the assembled DHM used for this work. The (yellow) SM fiber laser input is at the left, and the Ethernet camera (Baumer model TGX50-P) output (orange) is to the right.

A solid model of our optical concept is shown in Fig. 1(b), and a photograph of the assembled instrument in Fig. 1(c). The GRIN lenses (EFL = 0.92 mm, NA = 0.55) were mounted side-by-side in a black 3d-printed disk (25 mm diameter and 2 mm thick) and both the "GRIN disk" and the fiber-collimating lens (6 mm diameter) were tube-mounted (25 mm diameter). This "source assembly", with a total length of ≈25 mm, provides at its output the

Optics EXPRESS

desired pair of NA = 0.55 focal points spaced by 1 mm. The use of GRIN lenses thus allows a total "source assembly" volume of ≤ 1 cubic inch. Moreover, being enclosed in a short tube, the source assembly is very stable, and the over-illumination of the GRIN lens pair by a collimated beam eliminates any need for alignment of the GRIN disk. As centering the camera on the source assembly tube is also trivial, there are no difficult alignment steps involved. The only degrees of freedom are then the distances from the detector array to the planes of the sample and the GRIN foci, *s* and *f*, respectively (Fig. 1). With *f* ≈25 mm, the entire microscope is also quite compact, with a total system length of ≈10 cm in Fig. 1(c), roughly half that being due to the camera. In our lab setup, the camera distance is adjustable by means of a translation stage, but the stage is not needed in deployable units.

Image reconstruction was by means of direct propagation from the hologram plane after applying Fourier filtering [7,29], using either the Koala (LynceeTec) software package [30] or a custom MATLAB routine. The short spacings involved introduce some geometric distortion of the fringes (variable spacing and slight curvature), which is further complicated by passage through the sample media. Best reconstruction thus required subtraction of a reference hologram [31], which was produced either by imaging through an empty sample chamber or, in the case of a dilute sample with moving objects, choosing a single time point as a reference. The aberration phase map obtained from the reference-frame reconstruction was low-pass filtered and propagated back to the CCD plane for automatic subtraction from all of the holograms in an observation sequence. The aberration-corrected holograms were then directly propagated within Koala or MATLAB to yield image cubes. Holographic images were typically acquired continuously at 7 - 15 frames per second, and reconstructed in real-time (Koala), or close to real time (MATLAB) with standard Dell computers.

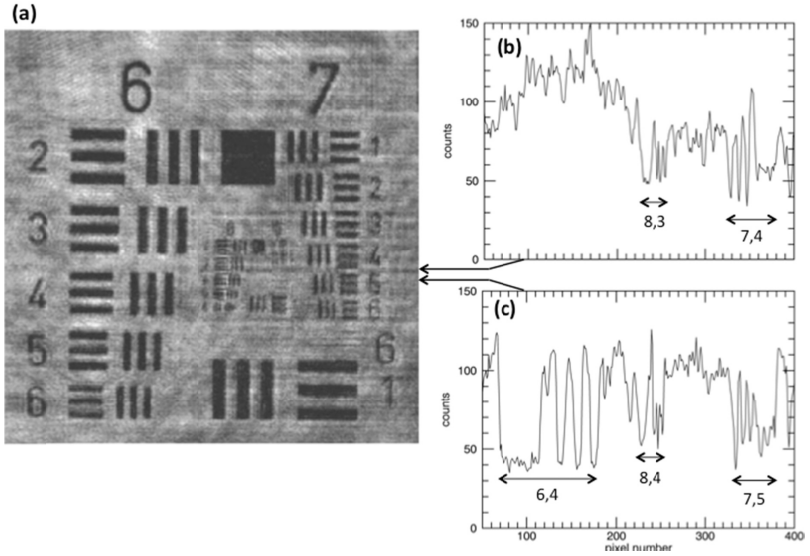

Fig. 2. (a) Reconstructed image of the central region of an Air Force target acquired with our DHM, (b) horizontal crosscut through the image intersecting target elements 8,3 and 7,4, and (c) horizontal crosscut through elements 6,4, 8,4 and 7,5. Arrows show the crosscut locations.

Figure 2 (a) shows a reconstructed image of an Air Force target that was acquired with the DHM of Fig. 1 (c) and the direct reconstruction procedure described. As the figure shows, this system resolves all of the elements of group 7 on an Air Force target and roughly half those in group 8. Note that the greyish, non-uniform background that extends across the image is due to the out-of-focus laterally-shifted image of the large outer opaque elements in

Optics EXPRESS

the extended Air Force target in the complementary image. This background structure would be much reduced if these larger-scale opaque structures did not surround the region of interest, as will be the case for biological targets. For this reason, Fig. 2(a) is far from a best case. Figures 2(b) and 2(c) shows two horizontal cross-cuts through the image of Fig. 2(a), where it can be seen that the vertical bars in element 3 of group 8 show fairly deep modulation, while element 4 of group 8 has a reduced fractional modulation, and is closer to the background fluctuation level near these elements. With line widths in the two cases of 1.55 and 1.38 μm, respectively, and allowing for the fact that some residual astigmatism and background contamination may be present in the image, in rough terms this demonstrates an ability to resolve features (line widths) down to ~1.5 μm. This is roughly as expected, as a source NA of approximately 0.17 for s ≈20 mm yields an expected resolution of ≈1.2 μm. Moreover, as all instrumental parameters and correction techniques available have not yet been fully explored or exploited (in particular, the integral C-mount on the front of the camera constrained the source-detector distance to be larger than the C-mount length), and as the mottled background due to the second beam is significant for the case of Air Force targets, the ultimate performance of this approach has likely not yet been reached.

With no optical elements between the GRIN foci and the camera, the depth of field extends essentially from the GRIN focal plane to the detector plane, with the resolution degrading from ≈1.5 μm at our sample location to 3.45 μm (the camera pixel size) at the detector plane. This extended depth of field was verified by translating the sample along the optical axis as much as allowed by the GRIN disk assembly and the camera C-mount, with sample motions over a range of ≈6 mm yielding similar performances. As to the field of view, similar triangles defined by the angle subtended by the array diameter, d, from the GRIN lens focus give

$$\frac{FOV}{d} = \frac{f - s}{f}. \tag{2}$$

With a 7 mm array, s ≈20 mm and f ≈25 mm yields FOV ≈1.4 mm. It should be possible to increase the FOV by removing the camera's C-mount to access smaller values of s. Finally, with the aberration-correction step described above, the resolution did not degrade noticeably across the image, e.g., Fig. 3(b).

3. Demonstration prokaryote observations

The ability to image and track prokaryotes was demonstrated on two test strains of different sizes, morphologies, and motility patterns. A sample chamber depth of 0.8 mm was made using optical quality cell culture wells (Electron Microscopy Sciences, part no. 70326-30) topped with a microscope slide or coverslip. The reference and object beams both passed through the sample. Hologram time series of 30-60 s at 7-15 frames per second were recorded and reconstructed as described. The resultant intensity images were median subtracted using Fiji [32], and the phase images cropped to exclude the edges, but otherwise unprocessed. Figures 3 (a) & (b) show single-plane amplitude and phase images of the larger bacterial strain (*Bacillus subtilis* ATCC 6051) that was fully resolved by our DHM. The cells were grown to mid-log phase in Lysogeny Broth (LB), and then immediately before imaging, diluted to a concentration of ~10^7/mL in motility medium (10 mM potassium phosphate, 10mM NaCl, 0.1mM EDTA, 0.1 mM glucose, pH 7.0). As is readily apparent in Visualization 1 and Visualization 2, the cells were highly motile, with a swimming speed of ~5-10 μm/s. For this larger bacterium, translational, rotational, bending and oscillatory motions are all very evident in Visualization 1 and Visualization 2. Some stationary cells, presumably adhering to the slide surfaces, are also seen.

Optics EXPRESS

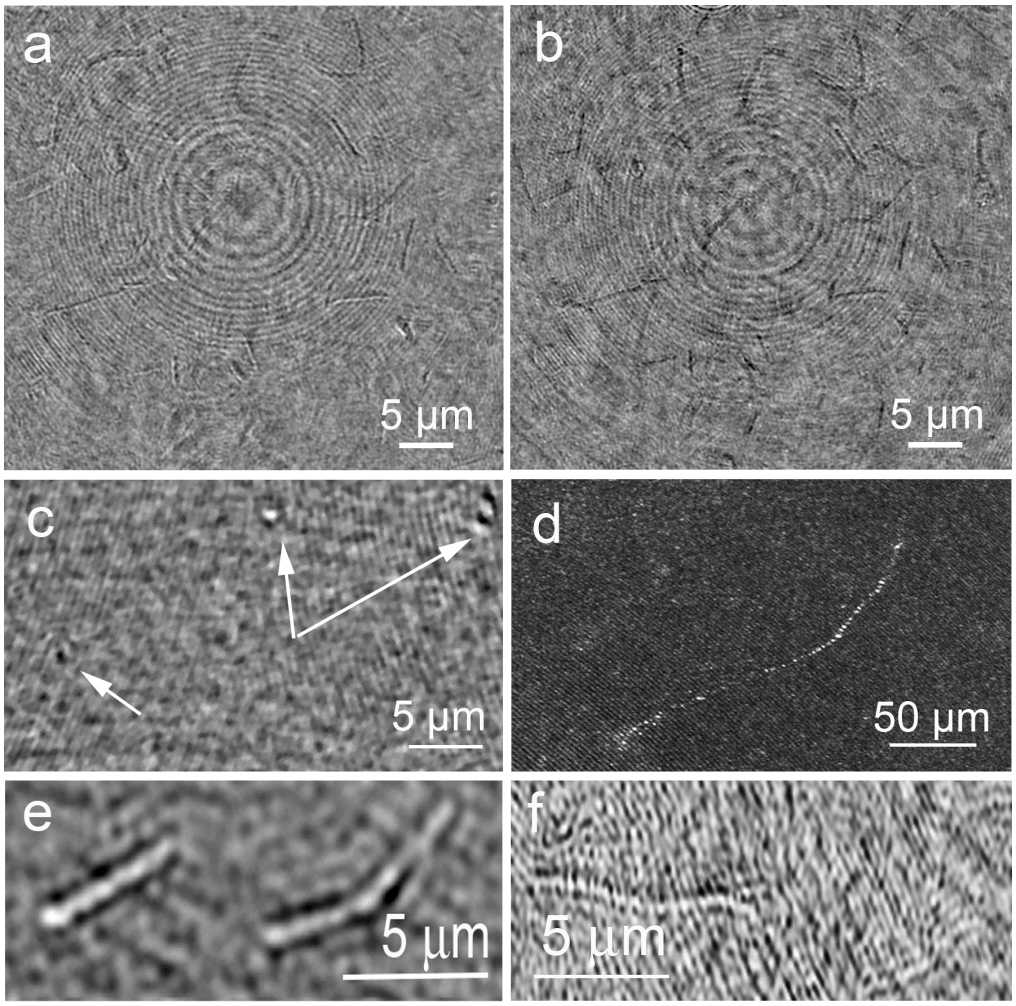

Fig. 3. Bacterial strains imaged with our lensless DHM. (a) *B. subtilis* in intensity (video shown in Visualization 1). (b) *B. subtilis* in phase (video in Visualization 2). (c) *Colwellia* in intensity (video in Visualization 3; a *Colwellia* phase video is shown in Visualization 4). The arrows indicate cells in or near focus. (d) A *Colwellia* time track. (e) Zoomed-in image of *B. subtilis* in a 100 µm deep chamber. (f) Zoomed in image of *B. subtilis* in an 800 µm deep chamber.

Next, the ability to detect unresolved cells in dilute solutions was demonstrated using a smaller bacterial test species. For this we used the marine psychrophile *Colwellia psychrerythraea* strain 34H, which measures approximately 1 x 0.5 µm and demonstrates rapid motility (up to 100 µm/s) [33]. The cells were maintained in ½ strength Marine Broth (Difco) at 6 °C, and diluted into the same culture medium for imaging. Their existence and motility was readily observed - when in focus, the cells appeared as bright spots in both intensity and phase. Figure 3(c) shows a single-plane amplitude reconstruction of organisms at a density of ~10^7 cells/mL, and Fig. 3(d) shows a time track constructed from amplitude data. Visualization 3 and Visualization 4 show amplitude and phase videos of a single-plane reconstruction sequence, in which a number of cells are seen to move across the field, thus demonstrating that such a microscope can be used for remote life searches down to somewhat below the instrumental resolution.

Optics EXPRESS

The choice of 800 µm deep sample chambers represented a compromise between SNR and freedom of axial movement. While the instrument's performance did not degrade substantially through a thicker air path, the signal-to-noise ratio of a particle suspension at high particle densities is inversely proportional to the product of the particle number density and the sample chamber depth [34]. Figures 3(e) and 3(f) shows a comparison of B. subtilis cells in the 800 µm deep chamber vs. cells in a chamber 100 µm deep, illustrating the increased contrast seen with thinner samples. If only 2-dimensional images are required, thinner chambers can be employed.

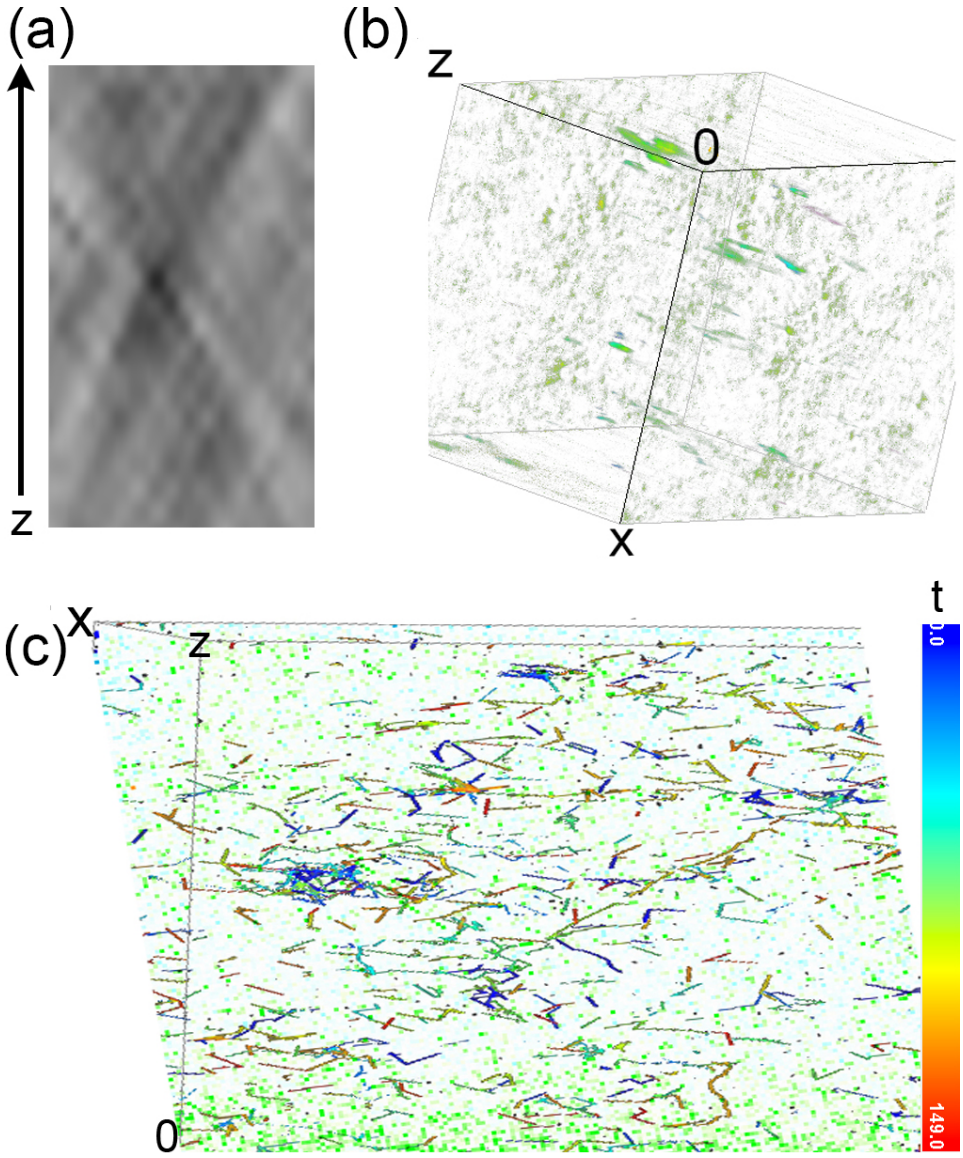

Fig. 4. 3D visualizations. 4a) xz image showing a cross section through the reconstructed PSF of a *B. subtilis* cell. (b) Image of *B. subtilis* culture at a single time. Individual cells can be identified by their extended PSFs. (c) 3D tracks of 30 s of cell motion of a Colwellia culture. Cells were identified using a maximum intensity projection. Non-motile cells (green) clustered near z = 0, while trajectories of motile cells spanned the volume. Time is color-coded.

Optics EXPRESS

The resolution obtained in all three dimensions, and the ability to track essentially unrestrained axial motion, may be appreciated by examining 4-dimensional data sets. Reconstructions in amplitude and phase were performed every 1.2 μm through the depth of the sample, permitting a three-dimensional view of the organism concentration and activity. Figure 4(a) shows an xz image of a single B. subtilis cell, illustrating the conical spread of the image along the z-axis (the propagation direction). Figure 4(b) shows a thresholded image of the entire volume of the *B. subtilis* sample. The spread of the individual cells along z can again be discerned. To achieve a resolution in z comparable to that seen in x and y, the point spread functions of the individual cells must be fitted to obtain the best focus. Figure 4(c) presents the maximum intensity projections of the video data across 30s of a recording of the Colwellia culture. It can be seen in both Figs. 4(b) and 4(c) that many of the cells in this culture were non-motile and clustered near the two surfaces of the slide. However, a significant density of live cells moving rapidly in x,y, and z can be seen between the chamber boundaries.

4. Summary

As demonstrated here, combining high-resolution, large depth of field and FOV, compactness, low weight (~100 gm for the optical system), robustness, and high data compression with real-time imaging and reconstruction is quite practicable with the GRIN-based approach described herein. Moreover, it is expected that the ultimate performance of this approach has not yet been reached. Other approaches to lensless digital holographic microscopy optimized for different applications exist, but the compact system described here is aimed at field and robotic use, and combines direct amplitude and phase imaging with tracking of microorganisms in dilute samples taken from bodies of water in remote environments. Especially intriguing in this regard is the possibility of space deployment. For autonomous deployment, the next steps beyond system optimization are miniaturization of the associated electronics and making them resistant to the required environmental conditions (i.e. temperature extremes and high pressure). Further aberration correction steps as well as limits of performance remain to be investigated, and it will be necessary to customize and integrate an appropriate microfluidic system for sample collection, pre-concentration, and delivery. Finally, we note that beyond the specific application described here, the use of GRIN lenses to provide a compact array of coherent point sources of light should have further applicability.

Funding

NASA Jet Propulsion Laboratory; Gordon and Betty Moore Foundation (4037, 4038).

Acknowledgments

Part of this work was carried out at the Jet Propulsion Laboratory, California Institute of Technology, under contract with NASA. We thank J. Deming (UW) for providing the *Colwellia* strain, and S. Rider (Caltech) for assistance with mechanical engineering.